Mechanical Computation in Neurons

Laishram J.[1], Avossa D.[1], Shahapure R.[1] & Torre V.[1,2] *

[1]*International School for Advanced Studies (SISSA-ISAS), Trieste, Italy.* [2]*Italian Institute of Technology, ISAS Unit, Italy.*

* Corresponding author:
Vincent Torre
Scuola Superiore di Studi Avanzati (SISSA)
P1-03b, Ed. Q1, AREA SCIENCE PARK
S.S.14, Km163,5
34012 Basovizza (TS)
ITALY
Email address: torre@sissa.it
Tel: +39 040 3756 513
Fax: +39 040 3756 502 /513

ABSTRACT

Growth cones are the main motile structures located at the tip of neurites and are composed of a lamellipodium from which thin filopodia emerge. In this manuscript, we analyze the kinetics and dynamics of growth cones with the aim to understand two major issues: firstly, the strategy used by filopodia and lamellipodia during their exploration and navigation; secondly, what kind of mechanical problems neurons need to solve during their operation. In the developing nervous system and in the adult brain, neurons constantly need to solve mechanical problems. Growth cones must decide how to explore the environment and in which direction to grow; they also need to establish the appropriate contacts, to avoid obstacles and to determine how much force to exert. Here we show that in sparse cultures, filopodia grow and retract following statistical patterns, nearly optimal for an efficient exploration of the environment. In a dense culture, filopodia exploration is still present although significantly reduced. Analysis on 1271, 6432 and 185 pairs of filopodia of DRG, PC12 and Hippocampal neurons respectively showed that the correlation coefficient $|\rho|$ of the growth of more than 50% of filopodia pairs was larger than 0.15. From a computational point of view, filopodia and lamellipodia motion can be described by a random process in which errors are corrected by efficient feedback loops. The present manuscript argues that neurons not only process sensory signals, but also solve mechanical problems throughout their entire lifespan, from the early stages of embryogenesis to adulthood.

Keywords: Mechanical computation; growth cone motion; growth cone exploration; obstacle avoidance; obstacle removal

INTRODUCTION

Processing of sensory inputs and its transformation into appropriate motor outputs is a key function of neuronal networks in all living species. A major goal of contemporary neuroscience is to understand this processing at a functional and molecular level. Similarly to electronic devices, neurons process sensory signals and information as electrical signals, but they are also living entities able to move. Indeed, neurons can explore the environment and migrate to destinations that are several microns, even millimeters, away from their original location (Dai and Sheetz, 1995; Atilgan et al., 2006; Solecki et al., 2006; Ghashghaei et al., 2007). Neuronal growth cones are the major motile structures located at the tip of dendrites and axons (Bray et al., 1978; Goodman, 1996; Song and Poo, 2001; Gordon-Weeks, 2004; Duncan et al., 2008), and are composed of a lamellipodium from which thin filopodia emerge (Pollard et al., 2000; Grunwald and Klein, 2002; Guan and Rao, 2003; Huber et al., 2003). The motion of filopodia and lamellipodia plays a major role in morphogenesis and neuronal differentiation: the exploratory motion of filopodia allows neurons to find the correct target and to establish the appropriate synaptic connections. Their motion has been analyzed and characterized to some extent by time lapse microscopy (Aletta and Greene, 1988; Gomez and Letourneau, 1994; Dent and Kalil, 2001; Baker et al., 2003; Baker and Macagno, 2007; Galbraith et al., 2007; Mongiu et al., 2007).

Growth cones contain a variety of adhesion molecules and receptors to guidance molecules (Bustamante et al., 2000; Yamagata et al., 2003; Huber et al., 2003; Curinga and Smith, 2007; Cline and Haas, 2008); a sophisticated intracellular biochemical machinery couples these receptors to the cytoskeleton (Gallo and Letourneau, 2000; Song and Poo, 2001; Gordon-Weeks, 2004) which is primarily composed of actin filaments and microtubules. Filopodia are usually composed of several bundles of actin filaments and occasionally of some microtubules (Howard, 2001, Schaefer et al., 2002). Growth cone membrane receptors detect guidance molecules (Nicholls et al., 2001) through a process commonly referred to as "pathfinding" which involves growth cone navigation along a gradient of a diffusible factor.

Mechanical properties of cytoskeletal components are usually quantified by measuring their persistence length, λ_p, defined as the length over which correlations of the motions between the tip and the end are lost (Howard, 2001). Cytoskeletal components with a length L such that $L/\lambda_p \ll 1$, move like rigid sticks and the motions of their tip and base are highly correlated. The value λ_p of actin filaments is 18±1 µm when stabilized with phalloidin and 9±0.5 µm in non-stabilized conditions (Isambert et al., 1995), while microtubules are more rigid with values of λ_p varying from 110 to 5035 µm (Pampaloni et al., 2006).

In this manuscript, we analyze the kinetics and dynamics of growth cones with the aim to understand two major issues: firstly, the strategy used by filopodia and lamellipodia during their exploration and navigation; secondly, what kind of mechanical problems neurons need to solve during their operation. In the developing nervous system - during neuronal differentiation and migration -, and in the adult brain - during memory formation and consolidation - , neurons have the constant necessity to solve mechanical problems: growth cones need to explore the environment, establish the appropriate contacts, avoid obstacles, decide in which direction to grow and how much force to exert. The present manuscript argues that neurons not only process information, but continuously solve mechanical problems throughout their entire lifespan, from the early stages of embryogenesis to adulthood.

METHODS

CELL CULTURE

Dorsal Root Ganglia (DRG) neurons were prepared from Wistar rats (P10-P12), anesthetized with CO_2 and sacrificed by decapitation (in accordance with the Italian Animal Welfare Act and approved by the Local Authority Veterinary Service), as previously described in Cojoc et al., (2007).

Dissociated cells were plated on poly-L-lysine (PLL, 0.5 µg/ml, Sigma) and Matrigel (BD Biosciences, Bedford, MA, USA) -coated coverslips in Neurobasal medium (Invitrogen) containing 10% fetal bovine serum (FBS, Sigma) and 100 ng/ml nerve growth factor (NGF, Alomone, Israel) at a density of 10^4 cells/ml (corresponding to ~2000 cells/cm^2).

PC12 cells were grown in RPMI (Invitrogen) supplemented with 10% horse serum (Sigma) and 5% FBS. The cells were plated on PLL and Matrigel coated glass coverslips in RPMI medium supplemented with 5% horse serum (Sigma) and 2.5% FBS at a density of 10^4 cells/ml (corresponding to ~2000 cells/cm^2). To induce differentiation into sympathetic neurons, 100 ng/ml NGF was added to the culture.

Hippocampal neurons were isolated from P0-P2 rats as previously described in Bonifazi et al., (2005). Cells were plated on polyornithine (Sigma)/matrigel-coated coverslips at a density of 8×10^5 cells/cm^2 and maintained in Minimal Essential Medium with Earle's salts (Invitrogen) supplemented with 5% fetal calf serum, 0.5% D-glucose, 14 mM Hepes, 0.1 mg/ml apo-transferrin, 30 µg/ml insulin, 0.1 µg/ml D-biotin, 1 mM Vit.B12, and 2 µg/ml gentamycin (all supplements were purchased from Sigma). 48 hours after plating, 5 µM cytosine-β-D-arabinofuranoside (Ara-C) was added to the culture medium, in order to block glial cell proliferation. Medium change was performed twice a week.

All neuronal cultures were kept in an incubator providing a controlled level of CO_2 (5%), temperature (37°C) and moisture (95%). DRG and PC12 neuronal cultures were used for imaging 20-30 hours after plating, while hippocampal cultures were used after two weeks in culture.

LIVE IMAGING, CELL TRANSFECTION

Differential interference contrast (DIC) images of moving DRG growth cones were obtained with a Leica DMIR2 confocal microscope (Leica Microsystems GmbH, Germany), equipped with a Diode laser emitting at 405 nm, and Ar/ArKr (at 488 nm), He/Ne (at 543/594 nm), and He/Ne (at 633 nm) lasers. Coverslips were placed into a chamber and kept at 37ºC and 5% CO_2 to minimize cell damage or death during live recording. The Ar/ArKr laser was used as a light source set at 11% of its maximal power so to reduce neuronal damage. Stacks of four images (set in DIC configuration) at different focal planes (0, 1, 2 and 3 µm above the glass where the neurons were plated) were acquired with a 63×, 1.4 NA oil immersion objective every 5-10 seconds, for 12 to 35 minutes. Time lapse movies of acquired images are shown in the Supplementary Information material: exploring filopodia in SI 1 and a moving lamellipodium in SI 2. The growth cone is a 3D structure because filopodia and lamellipodia can move by some microns along the z-axis and their three dimensional (3D) motion was recovered using an operator assisted program (see below).

Hippocampal neurons were transfected with pEGFP-N1 (CloneTech, Palo Alto, CA, USA), a plasmid encoding for enhanced green fluorescent protein (EGFP), after 8 to 11 days *in vitro* (DIV) using the Ca^{2+}-phosphate method (Köhrmann et al., 1999) and live imaging of moving growth cones was performed 2-5 days after transfection. To determine the cell density, sister hippocampal cultures were immunolabeled with the anti-β tubulin III antibody TUJ (Covance, USA; 1:750 dilution) and counterstained with DAPI (Boehringer Mannheim GmBH, Germany; 1:1000 dilution) as previously described (Bonifazi et al., 2005). At the time point chosen for live imaging of growth cones, the total cell density was $9.60 \pm 1.1 \times 10^4$ cells/cm^2 and the neuron density was $5.70 \pm 0.8 \times 10^4$ neurons/cm^2.

DATA ANALYSIS

Filopodia were tracked by an operator assisted program and data were analyzed using MATLAB 7.1 (The MathWorks Inc. http://www.mathworks.com). For each filopodium i and for each frame n (n=1,…,N) of a growth cone, we determined the location of its base or starting point $s_i(x,y,z,n)$ and the location of its tip or end point $e_i(x,y,z,n)$. Figure 1A illustrates a 3D rendering of the set of $s_i(x,y,z,n)$ in red and the set of $e_i(x,y,z,n)$ in black for a DRG growth cone. When these points are projected on the (x,y) plane, they are distributed over a portion of a circular sector with inner and outer radii R and R+A respectively and a central angle θ (Fig. 1B). The z resolution was equal to the distance between different focal planes, i.e. 1 µm. A suitable program combined the information obtained at each focal plane and the 3D backbone of each filopodium was recovered for all frames so

that it was possible to follow its motion in the 3D space. The distance D at frame n, was defined as the distance between $s_i(x,y,z,n)$ and $e_i(x,y,z,n)$, and the filopodial length L, as the sum of distances between consecutive points making up the filopodium backbone. A filopodium emerging from a point where another one had previously disappeared was considered as a new filopodium. With this procedure, the length and orientation of all filopodia were recovered.

ESTIMATION OF EXPLORABLE AND EXPLORED SPACE

In order to quantify the exploratory behavior of growth cones in culture, we define two quantities: the explorable and the explored 3D free space around growth cones. The explorable 3D free space is an estimation of the 3D space that the growth cone could potentially explore and the explored 3D space is the 3D space which is actually explored by the growth cone at a given frame n.

As shown in Figure 1A and B, the starting and ending points of all filopodia of DRG usually lie on the perimeter of a circular sector with inner radius R and an outer radius R+A, where R corresponds approximately to the radius of the growth cone and A is the maximal length of filopodia. If C is the centre of this circular sector, (see Fig. 1B), filopodia starting and ending points cover approximately an angle θ. Therefore, the volume of the explored 3D space at frame n is defined as:

$$Free(n) = h \cdot \pi((R+A)^2 - R^2) \cdot \frac{\theta(n)}{2\pi}$$

where h is the maximal height to which the filopodium tip can arise, estimated to be 3 μm (Figs. 1-2). $\theta(n)$ depends on the frame n whereas R and A are assumed to be constant. The explorable 3D space *ExplFree* is the maximum value of *Free(n)* over the entire image sequence n=1,…,N and the fraction of explored free space at frame n is
Free(n)/ExplFree.

For Hippocampal neurons, the volume of the explorable free space around a growth cone is assumed to be

$$ExplDense = \frac{4}{3}\pi((R+A)^3 - R^3)$$

i.e. the volume of a sphere of radius R+A minus the volume of the sphere of radius R. In these cultures, the explored space $Dense_{cyl}(n)$ at frame n is defined in the following way: for each filopodia i, we consider the segment S_{in} joining the starting $s_i(x,y,z,n)$ and ending point $e_i(x,y,z,n)$ and draw the cylinder Cyl_{in} with axis S_{in} and radius R_{cyl}. The radius R_{cyl} is assumed to be the standard deviation of lateral filopodia fluctuations corresponding to approximately 1 μm as measured by video microscopy. The explored space at frame n, $Dense_{cyl}(n)$, is defined as $U_i\,Cyl_{in}$, where U is the union operator of Set Theory. Thus, the fraction of explorable free space at frame n is the ratio of the two volumes *Dense(n)* and *ExplDense*.
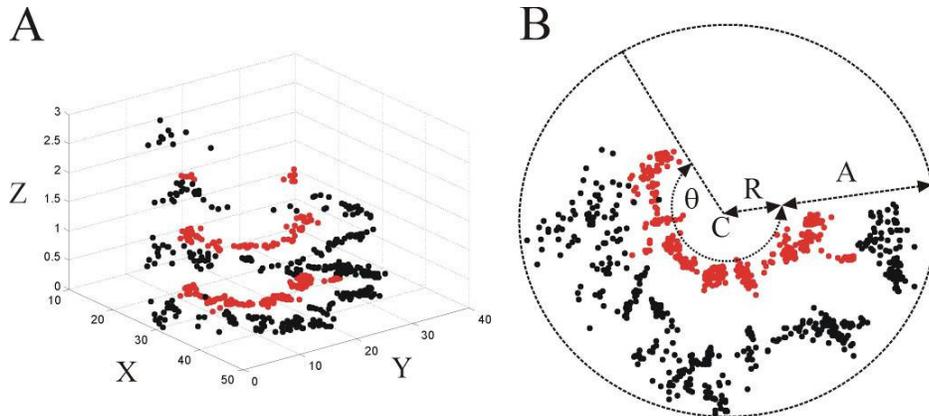
Fig. 1. Determination of the explorable and explored space around a growth cone. **A**: Red and black points are the starting $s_i(x,y,z,n)$ and end points $e_i(x,y,z,n)$ respectively of DRG filopodia identified during 10 minutes of observation. **B**: Determination of the explored free space by filopodia of a growth cone in a free environment, i.e. in a diluted culture.

CORRELATED AND ANTI-CORRELATED GROWTH

Given the 3D backbone of filopodia i and j at frame n, their mean lengths μ_i and μ_j over all frames were computed. If x_i is the set of lengths (at frames 1,…,N) of filopodium i and y_j is the set of corresponding lengths of filopodium j, the correlation coefficient ρ_{ij} between the length of filopodia i and j was computed as:

$$\rho_{ij} = \frac{E[(x-\mu_i)(y-\mu_j)]}{\sqrt{E[(x-\mu_i)^2] \cdot E[(y-\mu_j)^2]}}$$

where, E[·] is the average value of · computed over all frames 1,…,N; and μ_i and μ_j are the mean values of the lengths x_i and y_j over all frames 1,…,N.

ρ_{ij} could be positive or negative indicating correlated and anticorrelated growth respectively. In order to establish the existence of correlated or anticorrelated growth, two thresholds corresponding to ±0.15 and ±0.5 were considered (see Table 1). If the absolute value of ρ_{ij} was less than 0.15, the motion of filopodia was considered uncorrelated.

CONTACT FORMATION

Contact formation between neighboring growth cones was quantified by considering the number of formed contacts, lifetime and persistence. A contact between the two endpoints $e_i(x,y,z,n)$ and $e_j(x,y,z,n)$ of filopodia i and j is established at frame n if $e_i(x,y,z,n)$ and $e_j(x,y,z,n)$ coincided at frame n and for at least 10 subsequent frames. A previously formed contact was lost at frame m if $e_i(x,y,z,m)$ and $e_j(x,y,z,m)$ no longer coincided at frame m and for at least 10 subsequent frames.

OPTICAL TWEEZERS AND FORCE MEASUREMENTS

The optical tweezers setup was built as described in Cojoc et al., (2007). The dish containing the differentiating neurons and beads (1 μm diameter, PSI-1.0NH2; G.Kisker GbR, Steinfurt Germany) was placed on the inverted microscope stage which could be moved with a 3 axis piezoelectric nanocube (17 MAX 301, Melles Griot Inc., USA). The temperature of the dish was maintained at 37° C by a Peltier device. The bead position $\mathbf{x}=(x,y,z)$ was determined in the x,y plane with an accuracy of 10 nm using back focal plane (BFP) detection, which relies on the interference between forward scattered light from the bead and unscattered light. The BFP of the condenser was imaged onto a quadrant position detector (QPD) and the light was converted to differential outputs digitized at 20 kHz and low pass filtered at 5 kHz. Bead z position was determined using the Gouy phase shift effect (Neuman and Block, 2004; Rohrbach et al., 2004). The trap stiffness $\kappa_{x,y}=(k_x,k_y,k_z)$ and the detector sensitivity were calibrated using the power spectrum method. Detector sensitivity was also checked by measuring voltage signals originating from displacements of a bead stuck to the bottom of the coverslip with a nanopositioning device (the nanocube). The force exerted by the neurite $\mathbf{F_{neu}}$ was taken as equal to $-\mathbf{F_{trap}}$. When the absolute displacement of the bead $\mathbf{d}=(d_x,d_y,d_z)$ from its equilibrium position inside the trap was less than 400 nm, $\mathbf{F_{trap}}=(F_x,F_y,F_z)$ was calculated as $F_x=d_x k_x$, $F_y=d_y k_y$ and $F_z=d_z k_z$.

The velocity was obtained by numerical differentiation of the sampled position $(x(n),y(n),z(n))$ where n=1,…,N. Numerical differentiation was computed by convolution of the position with the derivative of a Gaussian filter A $\exp(-t^2/\sigma^2)$ with the unit area (Gaussian filtering).

RESULTS

The present manuscript is divided into two sections: an experimental section and a computational section. In the experimental section, we analyze several properties of the kinetics and dynamics of filopodia and lamellipodia motion. We have used three different types of neurons grown in culture: hippocampal neurons from the central nervous system, DRG neurons from the peripheral nervous system and PC12 cells differentiated into sympathetic neurons. In the present manuscript we show that, despite well-established differences (Joshi et al., 1985; Dennerll et al., 1989; Heidemann and Wirtz, 2004), all these neurons explore the surrounding environment with similar properties.

In the computational section, we model many of the results presented in the experimental section, with the aim of clarifying the notion of *mechanical computation* and formalize it in simple pseudo-codes.

EXPERIMENTAL SECTION

DRG neurons and PC12 cells were plated at low densities (2000 cells/cm^2) and were used after 20-30 hours in culture so to analyze growth cone motion in an environment where filopodia and lamellipodia could freely move. Hippocampal neurons, on the contrary, were plated at high densities (8×10^5 cells/cm^2) and cultivated for two weeks so to form a highly connected network.

KINETICS OF FILOPODIA MOTION

DRG and PC12 neurons were plated on glass coverslips and after 20-30 hours, neurites growing in different directions were observed. The kinetics of filopodia emerging from growth cones was analysed with time lapse DIC imaging (Fig. 2A). Images were taken at four optical sections corresponding to the plane of the coverslip (height of 0 µm) and to three other planes at a height of 1, 2 and 3 µm above the bottom of the coverslip (Fig. 2B). A stack of four images was acquired every 5-10 seconds for a total observation time varying from 8 to 30 minutes. DIC images acquired from 19 growth cones were analysed off line by an operator assisted program able to reconstruct the 3D profile of moving filopodia (see Methods). Filopodia lifted up and often appeared in focus some µm above the bottom of the coverslip (see Fig. 2B and SI 1 in Supplementary Information) and their tips visited locations at distances up to 16 µm from the lamellipodium edge.
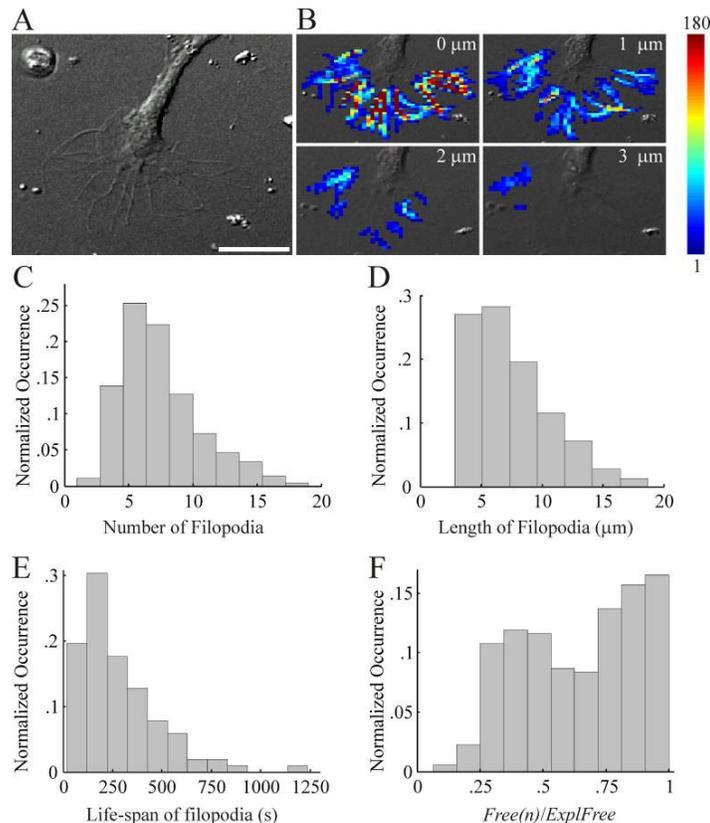
Fig. 2. Kinetics of filopodia from DRG growth cones. **A-B**: Density map of the region explored by filopodia from a DRG growth cone. In the color scale, red indicates highly visited voxels (180 times) whereas blue indicates less visited voxels (1 time). Scale bar: 10 µm. **C**: Normalized occurrence of the total number of filopodia from DRG growth cones. **D**: Normalized occurrence of length of DRG filopodia. **E**: Normalized occurrence of the life-span of DRG filopodia. **F**: Normalized occurrence fraction of the volume explored by a growth cone in a free environment calculated as *Free(n)/ExplFree*. Collected data from 19 DRG neuronal growth cones.

We analyzed the kinetics of filopodia from 19 DRG growth cones. Collected data show that the number of filopodia emerging from DRG growth cones was 7.3±3.4 filopodia per growth cone (range from 2 to 18 filopodia per growth cone) (Fig. 2C) and their length had an average value of 7.5±3.2 µm (range from 2.9 to 18.1 µm, n=19) (Fig. 2D). During the observation time, we identified several filopodia starting to grow and subsequently retracting completely. Exploring filopodia had a life time varying from just 1 to about 20 minutes (Fig. 2F). Other filopodia, after a period of exploration, stopped moving and appeared to stably adhere to the substrate.

We divided the space around a growth cone in cubic voxels of 1 µm. We computed how often each voxel was visited by a filopodium so to reconstruct the 3D profile of the space visited by filopodia: almost all voxels were visited at least once. As shown in Figure 2B, voxels at a height of 3 µm above the coverslip were occasionally visited by some filopodia.

The explorable free *ExplFree* and explored *Free(n)* 3D space around growth cones of DRG neurons was determined as described in the Methods. The value of *ExplFree* ranged from 1272 to 4671 µm^3 (n=19) with an average value of 3084±990 µm^3. At any time, the volume explored by the filopodia, *Free(n)*, varied from 187 to 4671 µm^3, with an average value of 1971±866 µm^3 . The fraction of the explored 3D space *Free(n)/ExplFree* had an average value of 66±24% (range from 6 to 100%, n=19) indicating that growth cones explored a significant fraction of the surrounding free space (Fig. 2F).

We reconstructed and tracked the 3D profile of each filopodium (see Methods), and calculated the ratio D/L, where D is defined as the distance between the filopodium tip and its base and L is the total filopodium length, computed as the sum of the distances between consecutive points making up the backbone of the filopodium. When the ratio D/L is close to 1, the filopodium is rigid, whereas values of D/L smaller than 1 characterize bending filopodia.
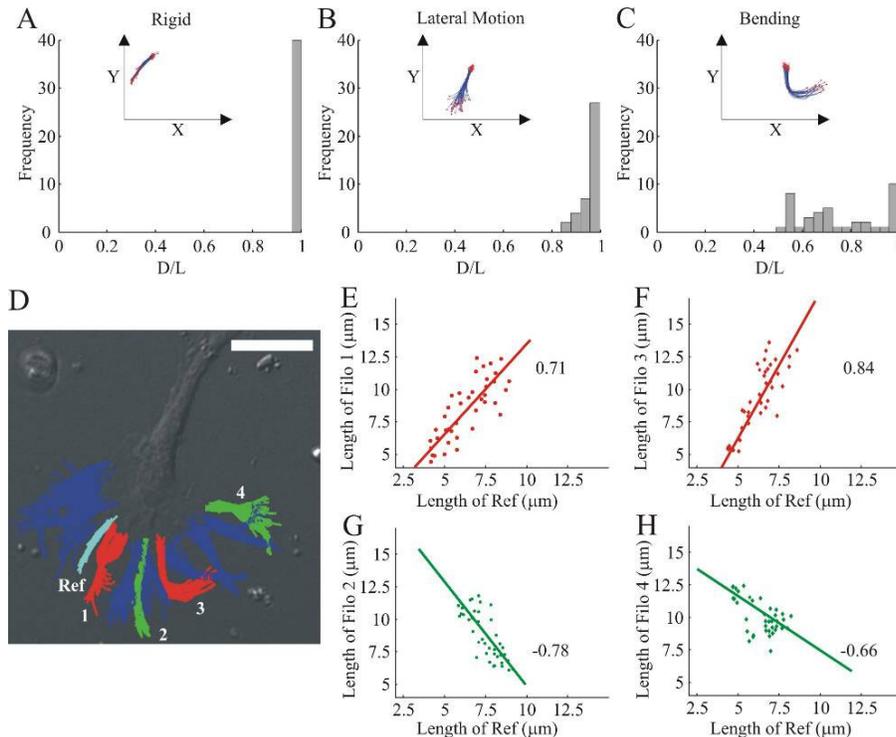
Fig. 3. Filopodia properties and correlated growth and retraction. **A-C**: Frequency distribution of the ratio D/L for three classes of filopodia respectively. Insets show the projection on the (X,Y) plane of a representative filopodium. **D**: 2D profile of filopodia emerging from a DRG growth cone superimposed to a DIC image of the growth cone. The filopodium marked in cyan is taken as reference. Scale bar: 10 µm. **E-H**: Cross-correlation between the length of the reference filopodium (in cyan) and the length of the two red filopodia indicated by 1 and 3 (E and F) and the length of the two green filopodia indicated by 2 and 4 (G and H). Changes in length of red and green filopodia were positively and negatively correlated to the changes in length of the filopodium marked in cyan, respectively. Changes in length of blue filopodia were not correlated.

The ratio D/L for several filopodia (29%) was very close to 1. These filopodia grew and/or retracted without changing the ratio D/L and behaved as rigid sticks emerging from the peripheral region of the growth cone (Fig. 3A). For other filopodia (18%) the ratio D/L varied between 0.8 and 1 and moved their tip laterally as if shaken at their base, possibly by shearing movements of the underlying actin filament network (Fig. 3B). For other filopodia (32%) the ratio D/L was less than 0.8, indicating a significant bending (Fig. 3C). Filopodia had at the most one bend and the ratio D/L did not change significantly during the observation time. The remaining filopodia (21% of all filopodia) could not be categorized into any of these classes because of their short lifespan. The average ratio computed over all filopodia fluctuated in time around 0.9 for all investigated growth cones.

During the recording time, new filopodia emerged and others completely retracted, therefore we investigated whether growth and retraction of neighboring filopodia were correlated (Fig. 3D-H). In all growth cones a specific filopodium was taken as reference such as that shown in cyan (Fig. 3D) and we analyzed whether other filopodia retracted or grew in synchrony. In the example shown in Fig. 3D when the cyan filopodium retracted, some neighboring filopodia (indicated in red) also retracted while other filopodia (indicated in green) grew. The correlation coefficient ρ between the length of the reference filopodium and the length of the red filopodia was 0.71 and 0.84 respectively, whereas the value of ρ with the two green filopodia was -0.78 and -0.66 respectively.

Table 1: Percentage of correlated filopodial growth in different neuronal growth cones

Type of neuron	Percentage of filopodia with (ρ is correlation coefficient) (A = Anticorrelated; C = Correlated)		
	Uncorrelated $|\rho|<0.15$	Moderately correlated $0.15 \leq |\rho| \leq 0.5$	Correlated $|\rho|<0.50$
DRG (n=19; 1271 pairs)	18.3	42.9 20.9 (A) + 22 (C)	38.8 14.1 (A) + 24.7 (C)
PC12 (n=6; 6432 pairs)	43.3	43.3 25.7 (A) + 17.6 (C)	13.4 1.4 (A) + 12 (C)
Hippocampal (n=7; 185 pairs)	38.4	39.8 28.2 (A) + 11.6 (C)	21.8 1.5 (A) + 20.3 (C)

We investigated the degree of correlated growth and retraction in 19 DRG, 6 PC12 and 7 hippocampal neuronal growth cones. Analysis on 1271, 6432 and 185 pairs of filopodia of DRG, PC12 and hippocampal neurons respectively showed that the correlation coefficient $|\rho|$ of the growth of more than 50% of filopodia pairs was larger than 0.15 (see Table 1). In DRG growth cones, 38.8% of these pairs had a value of $|\rho|$ larger than 0.5 and were classified as correlated, out of which 14.1% were anticorrelated and 24.7% correlated. 42.9% of the filopodia pairs were classified as moderately correlated (with correlation coefficient $0.15 \leq |\rho| \leq 0.5$), with 20.9% of the filopodia being moderately anticorrelated and 22% moderately correlated. The remaining 18.3% of these pairs had a correlation coefficient $|\rho|<0.15$ and were classified as not correlated. A similar degree of correlated growth was observed also in filopodia pairs of PC12 and hippocampal growth cones. These results indicate that growth and retraction of filopodia from the same growth cone are - to some extent - correlated, and when one filopodium grows, the other filopodium retracts.
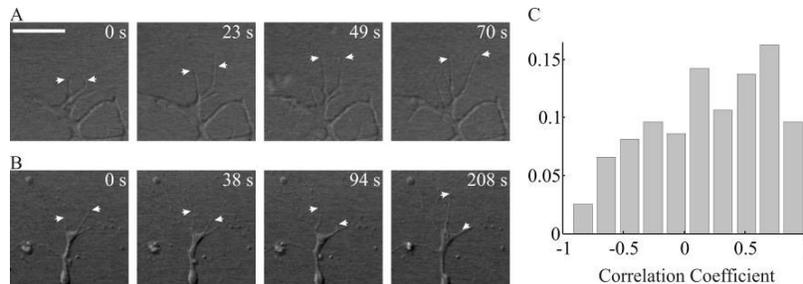
Fig. 4. Correlation between lengths of neighboring filopodia. **A** and **B** Selected frames of a growth cone with two filopodia (indicated by white arrows) growing in a correlated way (**A**) and growing in an anti-correlated way (**B**) Scale bar: 10 µm. **C**: Distribution of the coefficient of correlation ρ between 197 pairs of neighboring filopodia from the same growth cone. +1 indicates maximum correlation while -1 indicates maximum anti-correlation. The percentage of neighboring filopodia pairs with |ρ|>0.5 is 44.2%.

Having established that growth and retraction of filopodia from the same growth cone could be correlated and anti-correlated, we analysed in detail the degree of correlation between 197 pairs of neighboring filopodia from the same DRG growth cone. Two neighboring filopodia could grow simultaneously almost doubling their length within a minute (Fig. 4A). We also observed the opposite behavior (Fig. 4B): when one filopodium grew, a neighboring filopodium retracted (43/197) and, in some occasions (18/197) , it retracted completely.

Data collected from 197 of neighboring filopodia in DRG neuronal growth cones (Fig. 4C) respectively indicated a variable degree of correlated growth, with values of ρ ranging from -0.8 to 1. The fraction of pairs of neighboring filopodia showing a correlated growth with a value of |ρ| larger than 0.5 was 44.2%, similar to what was observed in pairs of filopodia - not necessarily neighboring - from the same growth cone, as shown in Table 1. Therefore, correlated growth or retraction does not necessarily depend on the proximity to the reference filopodium and often we observed significant correlations between distant filopodia. This orchestrated motor plan minimizes collisions between adjacent filopodia and provides an even exploration of the surrounding environment both in time and space. In addition, this motor plan allocates necessary metabolic resources - such as ATP molecules - in an efficient way and provides a possible recycling of G-actin monomers between polymerizing and depolymerizing actin filaments in neighboring filopodia. These observations allow us to understand the fine orchestration of filopodial motion underlying their mechanical computation.

FILOPODIA MOTION AND CONTACT FORMATION

Filopodia emerging from growth cones explore the environment in search of neurons in order to establish a physical contact. Therefore, we looked for pairs of neighboring growth cones and followed their exploratory motion and kinetics of contact formation. We observed two cases of contact formation between neighboring PC12 neuronal growth cones.
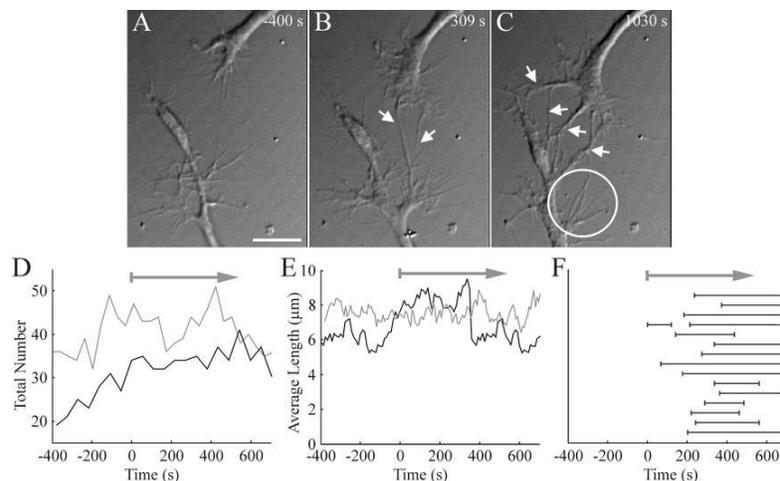
Fig. 5. Contact formation between two neighboring exploring PC12 growth cones. **A-C**: DIC images during contact formation. Time zero corresponds to the formation of the first contact. Scale bar: 10 µm. **D**: Total number of filopodia from the two growth cones during contact formation. The grey horizontal arrow indicates the period during which the contacts between growth cones were established. **E**: Time evolution of the average filopodia length. Data from two experiments. **F**: Time course of contact formation for one pair of growth cones. Arrows indicate the timing of the formation of physical contact and the arrow head indicates that the contact was also present at the end of the observation time.

Growth cones had between 20 and 50 exploring filopodia (Fig. 5A) and seven minutes after the start of the recording, two filopodia - from different growth cones - collided and established a permanent contact (Fig. 5B). Subsequently, several additional contacts were made (Fig. 5C) and then one growth cone retracted (shown within the white circle) without destroying the established contacts. Established contacts were usually stable and could be seen for several hours after image recording. Before establishing the contact, the total number of filopodia slightly increased (Fig. 5D) and after the formation of 2-5 contacts (white arrows), the total number of filopodia decreased. During the exploratory phase, contact formation and retraction, the average filopodia length remained stable with a value of 7.2±1.1 µm (range 3.5 to 9.5 µm) (Fig. 5E).

In one observation (see Fig. 5F), the number of contacts reached a maximum value of 15 contacts 400-650 seconds after the first contact was established, and 4 contacts were subsequently lost, but 11 out of 15 were present at the end of the observation time (10 minutes). One contact was interrupted but then quickly reformed. A large portion of exploring filopodia had a rather brief life varying from 1 to 6 minutes, but other filopodia explored for a longer time, up to 10-20 minutes.

FILOPODIA MOTION IN A DENSE CULTURE

Cultures of hippocampal neurons derived from neonatal rats were plated at high densities (8×10^5 cells/cm^2), and were grown for two weeks *in vitro* in serum-containing medium (see Methods section). In these conditions, glial cells rapidly proliferated and formed a cell monolayer on top of which neurons grew and became richly innervated (Goslin and Banker, 1998). To visualize neuronal growth cones, cultures were transfected with EGFP at 11 DIV and analyzed with time lapse confocal microscopy two days later (Fig. 6). To determine the cell density and the percentage of neurons, sister cultures were fixed and immunolabeled with the TUJ antibody which recognizes β tubulin III, a specific marker for neurons and DAPI staining for nuclei. The density of hippocampal cultures was quantified by counting the number of cells in an area of 100×100 µm^2 at the time of plating (n_{cover}) and after cultivation and DAPI staining (n_{DAPI}). In our experimental conditions, n_{cover} was 80±12 and n_{DAPI} was 25±15. The measured value of n_{DAPI} was about 2-8 times lower than n_{cover} because of cell death during cultivation. The total thickness of the culture was 50±15 µm. The average radius of the soma of these neurons was 7.4±2.2 µm and the measured volume of the dendritic tree was 5.4±1.3 times that of the cell body (unpublished data). Hence, the fraction of the volume occupied by the cells is between 37 to 79% and the free space around the growth cones is limited.
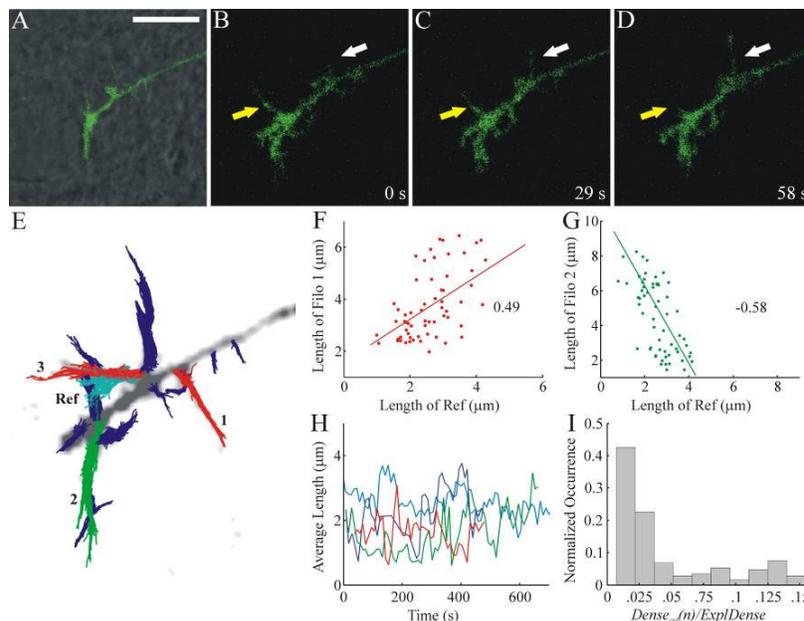
Fig. 6. Filopodia motion in dense neuronal cultures. **A-D**: Time lapse images of a growth cone from a hippocampal neuron transfected with EGFP. **A**: Overlay of a transmitted and fluorescent image. Scale bar: 10 µm. **B-D**: Example of negatively

correlated growth: the filopodium indicated by the yellow arrow retracted whereas the filopodium indicated by the white arrow grew. **E**: 2D profile of filopodia emerging from the same growth cone. The filopodium indicated in cyan is taken as the reference filopodium, 'Ref'. **F-G**: Cross-correlation between the length of filopodia indicated by the corresponding numbers in panel **E** and the reference filopodium, 'Ref' indicated in cyan. Each point indicates the length of the two filopodia at different observation times. The length of filopodia marked in red and green are positively and negatively correlated respectively to the length of the filopodium marked in cyan. The length of blue filopodia is not significantly correlated to the length of the reference filopodium. **H**: Time evolution of the average filopodia length for four hippocampal growth cones. **I**: Percentage of explored free space by filopodia in dense hippocampal cultures computed as $Dense_{cyl}(n)/ExplDense$. Data from 7 hippocampal neuronal growth cones.

Also in dense hippocampal cultures, filopodia grew and retracted within minutes (Fig. 6A-D). The motion of filopodia, however, was more restricted compared to that of filopodia from DRG neurons and filopodia primarily moved along specific directions (Fig. 6E) less occupied by other biological structures. The explorable free space $Dense_{cyl}$ and explored space $ExplDense$ were estimated as described in the Methods section. $ExplDense$ was estimated by assuming the radius of the growth cones to be 5 μm and the filopodia length, 3 μm (Fig. 6H). The average value of $ExplDense$ was 682±202 μm^3 (range from 514 to 944 μm^3; data from 7 hippocampal neuronal growth cones). As shown in Figure 6I, the fraction of explored free space ($Dense_{cyl}(n)/ExplDense$) was, on average, 4±4% ranging from 0 to 14% (n=7). The fraction of explored free space was significantly smaller than for DRG growth cones in culture where filopodia could move freely (Fig. 2D), indicating that filopodia exploration in dense hippocampal cultures is highly restricted.

The average tip velocity of hippocampal filopodia was 0.06±0.04 μm/s (n=7) for hippocampal neurons vs. 0.4±0.3 μm/s (n=19) for DRG neurons. The total number of filopodia emerging from growth cones of DRG neurons varied from 2 to 18, rarely exceeding 15; while in hippocampal growth cones, the total number of filopodia varied from 2 to 8, rarely exceeding 5. The length of filopodia varied between 1 and 11 μm and their average length was around 3 μm (3.1±0.9 μm, range from 1.5 to 6.4 μm) (Fig. 6H). Similarly to what observed for DRG growth cones, growth and retraction of neighboring filopodia was correlated: as shown in Figures 6B-D, when one filopodium retracted (yellow arrow), a neighboring filopodium grew (white arrow).The correlation coefficient ρ between the length of the reference filopodium (cyan in Fig. 6E) and that of the two red filopodia was 0.48 and 0.49 (Fig. 6F) whereas the value of ρ with the length of the green filopodium was -0.58 (Fig. 6G). The growth of blue filopodia was not correlated to that shown in cyan.

We investigated the degree of correlated growth and retraction in 185 pairs of neighboring filopodia from 7 growth cones (see Table 1). Of all these pairs, 21.8% had a correlation coefficient higher than 0.5 suggesting a strong correlated behavior (1.5% were anticorrelated and 20.3% were correlated) while 39.8% were moderately correlated (28.2% were moderately anticorrelated while 11.6% were moderately correlated). The remaining 38.4% had a value of |ρ|<0.15 and were considered not correlated. Therefore, we can conclude that filopodia growth and retraction is correlated also in dense hippocampal cultures. Correlated or anticorrelated growth or retraction was observed in pairs of filopodia emerging from the same growth cone and not necessarily from neighboring filopodia, as shown in Figures 6B-D.

DYNAMICS OF FILOPODIA AND LAMELLIPODIA MOTION

When a filopodium collides with an obstacle, it probes its chemical properties and mechanical resistance. Exploring filopodia can collide with an obstacle during their protrusion when polymerizing actin filaments push the membrane forward. Filopodia can also hit the obstacle from the side leading to a lateral collision. By using optical tweezers and appropriate detectors, it is possible to measure the bead position $\mathbf{x}=(x,y,z)$, its velocity $\mathbf{v}= (v_x,v_y,v_z)$ and the force $\mathbf{F}= (F_x,F_y,F_z)$ exerted on it by growth cones (Cojoc et al., 2007). Figure 7A shows the three components F_x, F_y and F_z of the exerted force $\mathbf{F}$ and Figure 7B the trajectory of the displaced bead in the 3D space. The force exerted by an isolated filopodium never exceeded 2 pN, neither during lateral collisions nor during protrusions.

While exploring, lamellipodia could displace encountered obstacles. During some collisions, the force developed primarily in one direction but, more often, the force $\mathbf{F}$ changed in all three

orthogonal directions (Fig. 7A) and the bead described a complex trajectory (Fig. 7B). In these experiments (n=13), it was possible to measure simultaneously the force **F** exerted by the lamellipodium on the bead and its velocity **v**. From these two vectorial quantities, the exerted power was obtained by their scalar product **F·v** (Fig. 7C) and the instantaneous power per unit area of the bead could reach values close to 10^{-17} Watt μm^{-2} as in the experiment analysed in Figure 7. When data were considered at a bandwidth up to 30 Hz, we measured power up to 10^{-16} Watt μm^{-2} in lamellipodia which were moving vigorously.
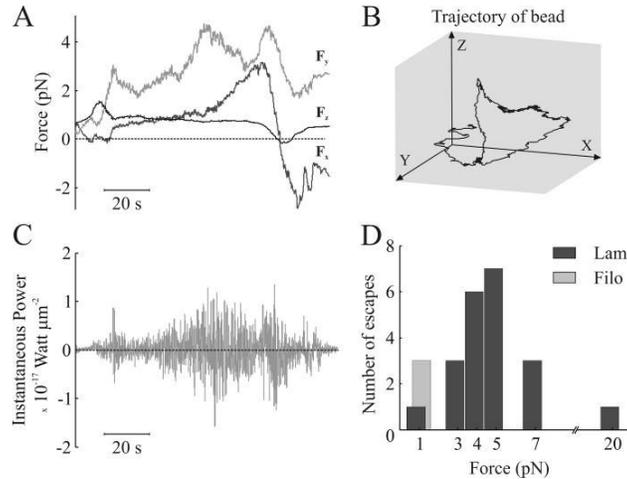
Fig. 7. Force exerted by filopodia and lamellipodia of DRG growth cones. **A**: The three components of the force F_x, F_y and F_z exerted by a lamellipodium during a collision with a trapped bead smoothed at 10 Hz. Forces measured with an optical tweezer (see Methods). **B**: Trajectory of the bead during its collision with the lamellipodium. The bead coordinates are detected using a quadrant position detector positioned on the back focal plane (see Methods). **C**: Instantaneous power produced by the lamellipodium per unit area of the bead during the collision, computed as **F·v**, where **F**=(F_x,F_y,F_z) is the force exerted on the bead and **v**=(v_x,v_y,v_z) is the bead velocity. **D**: Histogram of collisions between trapped beads and filopodia (pale grey) and lamellipodia (dark grey) resulting with the displacement of the bead out of the optical trap, as a function of maximal trapping force. (Lam=lamellipodia, Filo=filopodia).

We counted the number of collisions (N= 24) in which filopodia and lamellipodia displaced the bead out of the optical trap. Beads were trapped with different laser powers so to vary the stiffness of the encountered obstacles and almost one hundred collisions were observed. Filopodia are less suitable than lamellipodia to displace obstacles: indeed only occasionally (3/24), an isolated filopodium was able to move a bead out of its trap: in all these cases, the maximal trapping force F_{max} was 1 pN (Fig. 7D). A trapping force of 1 pN is very small and corresponds to an almost negligible stiffness. When F_{max} was increased to 3 pN, we never observed a filopodium displacing a bead out of its trap and we concluded that isolated filopodia cannot efficiently displace obstacles even those with a low stiffness. In contrast, lamellipodia could displace beads from the trap even when the maximum trapping force was 20 pN (Fig. 7D). In these experiments, the bead diameter was 1 μm and therefore the measured maximal pressure and power per unit area of the bead was 20 pN μm^{-2} and 10^{-16} Watt μm^{-2}. If lamellipodia exert maximal pressure of the order of 20 pN μm^{-2}, the total force exerted by a lamellipodium on an obstacle, such as debris or a cell intruding in the path towards its desired destination will depend on its size. Therefore, lamellipodia are expected to exert larger forces on larger obstacles, possibly up to hundreds of pN.

A. Sterotyped Filopodia Behavior   B. Sterotyped Lamellipodia Behavior
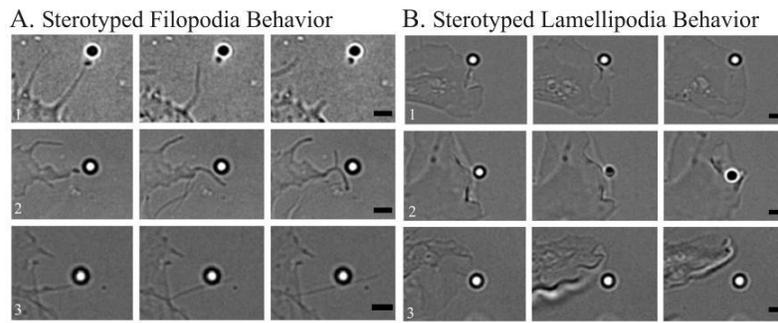
Fig. 8. Stereotyped filopodia (**A**) and lamellipodia (**B**) behaviors in the presence of an obstacle mimicked by a silica bead of 1 µm diameter trapped with an optical tweezers. See text for an illustration of these behaviors. Scale bar: 2 µm.

When filopodia and lamellipodia encounter obstacles, they seem to follow stereotyped patterns. An isolated filopodium colliding with an obstacle exhibits three possible behaviors illustrated in Figure 8A: 1) it can collide with the obstacle and then fully retract (Fig. 8A1); 2) after the initial collision the filopodium partially retracts branching new filopodia in one and even two different directions (Fig. 8A2); 3) a light collision with the obstacle, after which the filopodium continues its growth or exploration (Fig. 8A3). We have analysed the probability of these three different behaviors as a function of the obstacle stiffness, i.e. its resistance to an exerted force. Data collected from 98 experiments show that strong collisions with a stiff obstacle were usually followed by a retraction. Similarly, when a lamellipodium encounters an obstacle, it reacts in three possible ways: 1) it collides with the obstacle but continues its motion by growing underneath it (Fig. 8B1); 2) it can collide with the obstacle in a "shovel like" fashion, displacing it rearwards (Fig. 8B2); 3) it can retract (Fig. 8B3). We have analysed the probability of these three different behaviors as a function of the obstacle stiffness, but we could not find any clear correlation between stiffness and lamellipodium behavior.

The results illustrated in Figures 7 and 8 show several dynamical properties of filopodia and lamellipodia. Firstly, filopodia cannot displace obstacles and act primarily as exploring sensors but lamellipodia, in contrast, are able to efficiently displace obstacles. Secondly, lamellipodia can develop a power per unit area up to 10^{-16} Watt μm^{-2} and this power must be properly used and maintained. Thirdly, when encountering obstacles, filopodia and lamellipodia react displaying a stereotyped behavior. In the next section, it is argued that these stereotyped reactions are essential components of mechanical computation.

COMPUTATIONAL SECTION

This section aims to establish a computational framework in order to understand the kinetics and dynamics of filopodia and lamellipodia. We follow the classical view that a computation is the solution to a problem, which can be solved by the most general and simple computing device, i.e. the Turing Machine (Hopcroft et al., 2006). Therefore, we will use a computational approach by creating a pseudo-code (a program) able to solve mechanical problems.

As we have seen in the previous section, randomness is a major feature of filopodia and lamellipodia kinetics and dynamics. In growth cones, however, the random exploration of the environment is coupled to a variety of feedback loops. These feedback loops are formed by: i) the factors controlling axon growth and guidance molecules such as neurotrophins, morphogens and molecules of extracellular matrix (Curinga and Smith, 2007); ii) the receptors present on the growth cone membrane which detect these factors; iii) the consequent activation of a signaling cascade within the growth cone. These loops are responsible for the rapid formation of physical contacts when two filopodia tips with appropriate receptors meet (Fig. 5) or for the rapid retraction of a filopodium when a stiff obstacle is encountered (Fig. 8). They have been optimized by billions of years of evolution making the random search and exploration "smart" and "efficient".

The combination of a random exploration with efficient feedback loops that continuously correct errors provides the basis of what we propose to be *mechanical computation,* by which neurons establish their appropriate physical and chemical contacts, migrate to their final destinations, enlarge and/or prune spines and synapses. Let us see some examples of mechanical computations and how the combination of a random search and feedback loops can lead to the efficient solution of mechanical problems. Mechanical computations will be described as pseudo-codes for a probabilistic Turing Machine (Hopcroft et al., 2006), mixing random searches with feedback loops.

MECHANICAL COMPUTATION: OBSTACLE AVOIDANCE

For simplicity, let us consider an idealized filopodium tip moving on a square grid, with the origin (0,0) in the upper left corner. The filopodium tip starts at an initial point on line 0 (such as (0,13)) and its goal is to reach any point on line -20 avoiding the obstacles shown in Figure 9A. The pseudo-code able to perform this mechanical computation is:

> 1   *Move from (m,k) to (m,k+1)*
>   **If an obstacle is encountered, retract to (m,k)**
>   <u>and move with p=½ to to (m-1,k) or to (m+1,k)</u>
>   *Go to 1*

The program is composed of one simple reaction, i.e., the instruction to move, and one feedback loop, i.e., the instruction to retract if an obstacle is encountered (indicated by the bold lines) and by random searches (indicated by the underlined line).
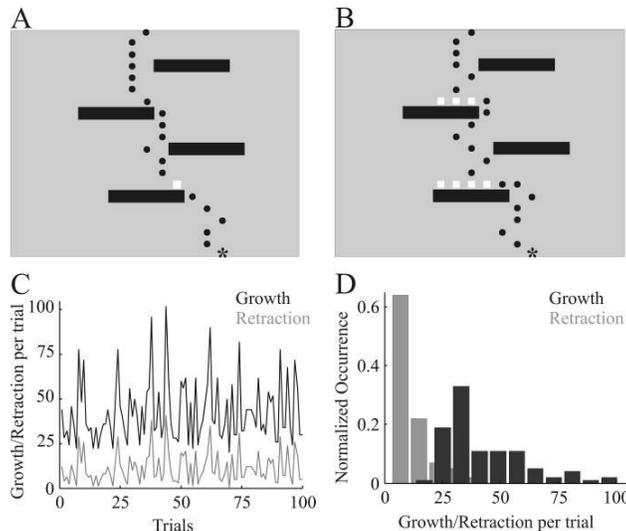
Fig. 9. Mechanical computation: Obstacle Avoidance. **A-B**: Two trajectories of a filopodium tip avoiding obstacles (black bars) and reaching the final destination (black star). **A** reproduces a fast trajectory with a low number of moves, whereas **B** reproduces a slow trajectory with several retractions and a high number of moves. Moves and retractions are denoted by black circles and white squares respectively. **C**: Number of growths (black trace) and retractions (grey trace) required to reach destination per trial. **D**: Normalized distribution of number of growths (black) and retractions (grey) per trial.

A filopodium tip following this program avoids obstacles and is able to reach its final destination (Fig. 9) following a simple trajectory with a limited number of retractions (Fig. 9A) or with a large number of growths and retractions (Fig. 9B). Black circles and white squares represent growth and retraction respectively while the black star represents the final destination in Figures 9A and 9B. The program - or the computation - is intrinsically probabilistic: the number of retractions (grey trace in Fig. 9C) and the number of steps (black trace in Fig. 9C) necessary to reach the final destination vary significantly from trial to trial from 20 to 100. As shown in Figure 9D, the distribution of number of growths (black) and of retractions (grey) had a long tail corresponding to the

trials in which the filopodium tip did not find immediately its way through the obstacles and retracted before reaching its final destination (Fig. 9B). The computation can be made faster and more efficient by introducing a gradient of guidance molecules, as it will be shown in the next example.

MECHANICAL COMPUTATION: FORMATION OF PHYSICAL CONTACTS

Let us now consider two idealized growth cones each formed by two filopodia (Fig. 10A) so that when one filopodium grows the other one retracts (see Figs. 3 and 6). This correlated behavior can be formalized by assuming that the length of the two filopodia l_1 and l_2 satisfies the relation $l_1+l_2=L$ where L is a fixed length. We assume also that one filopodium has at its tip a receptor R_1, able to form a physical contact with the tip of a different filopodium with the same receptor R_1. Another filopodium has at its tip a different receptor R_2 which can form a physical contact with filopodia bearing at their tips the same receptor R_2. The exploratory motion of all these four filopodia is random but it is constrained by the condition that $l_1+l_2=L$. The mechanical computation to be solved is the formation of a physical contact between the filopodia tips with the same receptor R_i. The pseudo-program able to perform this mechanical computation is:

1   *The tip of filopodium 1 of growth cone 1 moves from (n_1,m_1) to (n_1+i,m_1+j) with probability $p_{i,j}$*
   The tip of filopodium 2 of growth cone 1 moves from (k_1,h_1) to (k_1+i,h_1+j) so that $l_{1,1}+l_{2,1}=L$
   The same for growth cone 2
   If filopodia tips with the same receptors meet in the same location go to 2
   Go to 1
2   **Formation of a physical contact**
   Stop

where, the parameters "i" and "j" are constrained to single grid jumps, i.e. i and j=[-1,0,1], so that single step horizontal, vertical and diagonal moves are allowed. The simple reactions/feedbacks and random searches are indicated in the same style as in the previous pseudo-program.
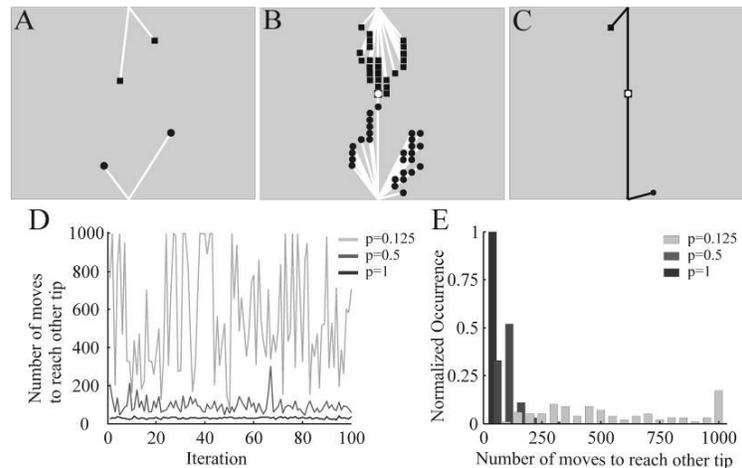
Fig. 10. Mechanical computation: Formation of Physical Contacts. **A**: Initial configuration of two idealized growth cones (black square and black circles) with two filopodia each. **B**: Representative configurations of the two growth cones before the formation of a physical contact. The total length of filopodia in each growth cone is constant. **C**: Final configuration, in which filopodia tips meet (white circle coinciding with black square). **D**: Number of steps required for formation of physical contact in different trials. When p=0.125, the search is completely random and the number of steps necessary to establish a physical contact is highly variable. When p=0.5, the search is biased by a chemical cue in the correct direction. When p=1, the search is completely deterministic and tips move straight towards each other. **E**: Normalized distribution of number of steps for p=0.125 (pale grey), p=0.5 (dark grey) and p=1 (black).

Given the initial configuration of two growth cones (Fig. 10A), the tips of the two filopodia in each growth cone move randomly (Fig. 10B) and after some iterations, a physical contact can be

established (Fig. 10C). Also in this case, the number of necessary steps varies significantly from trial to trial (Fig. 10D). When the search is completely probabilistic - i.e., there are no guidance molecules present and the probability $p_{i,j}$ is equal in all directions ($p=1/8=0.125$) - a physical contact is established after a high number of moves. The number of moves, however, can be substantially decreased by introducing guidance cues i.e, helping the two filopodia with the same receptors to meet more often. At each step, the probability $p_{i,j}$ of the filopodium tip bearing receptor R_i moving towards the tip of the filopodium bearing the same receptor R_i can be increased by introducing a guidance molecule. From a computational point of view, this is equivalent to increasing the probability to move towards the correct direction from p to p*, while the probability to move towards the other seven directions is reduced to (1-p*)/7. As shown in Figures 10D-E, the total number of moves required to establish a physical contact is substantially decreased when p*=1 (black trace) and p*=1/2 (dark grey trace) in comparison to the case where all p_{ij} are equal to 1/8 (pale grey trace). When p*=1, the search is completely deterministic and the physical contact is formed in a limited number of moves.

MECHANICAL COMPUTATION: OBSTACLE REMOVAL

Let us now consider a slightly more complicated mechanical computation: a lamellipodium besides retracting or avoiding obstacles also displaces them. At each cycle, the lamellipodium can exert a force $F_1 < F_2 < ... F_i < ... < F_n$. Obstacles have varying stiffness $S_1 < S_2 < ... S_j < ... < S_n$ (indicated by the numbers on the black/grey bars in Fig. 11A) and can be displaced when the lamellipodium exerts a force $F_i > S_j$. For this task, when an obstacle is encountered, the lamellipodium has to choose between two options: to retract towards or to advance and to exert a force F_i and see whether it will displace the obstacle. If the maximum force exerted by the lamellipodium is not strong enough to displace the obstacle, the lamellipodium will retract.
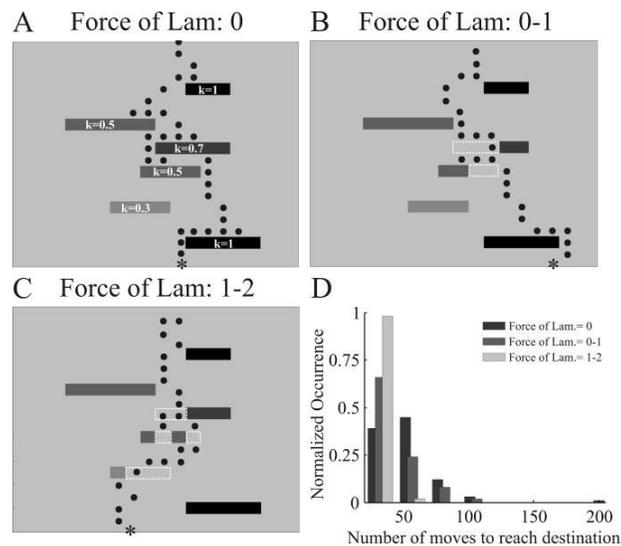
Fig. 11. Mechanical computation: Obstacle Avoidance and Removal (Lam stands for lamellipodium). **A**: Trajectory of a lamellipodium avoiding obstacles (represented by black bars) and reaching the final destination (black star), corresponding to line 20. Each obstacle has a stiffness ranging from 0 to 1, as indicated. **B-C**: Trajectories of a lamellipodium able to displace obstacles. The lamellipodium can exert forces varying from 0 to 1 (**B**), and from 1 to 2 (**C**). Force and stiffness are in the same arbitrary units. The lamellipodium can displace an obstacle and then it could retract, see some cases in **B** and **C**. Removed obstacles are shown as dotted white boxes. **D**: Normalized distribution of number of moves/steps necessary to reach the final destination when the lamellipodium does not exert a force (black), when it exerts a force varying from 0 to 1 (grey) and from 1 to 2 (pale grey).

As shown in Figure 11A, if the lamellipodium cannot exert any force, it has to navigate its way through the obstacles before finding its final destination. When the lamellipodium can exert forces up to 1 will displace objects with a stiffness lower than 1 (where the force and the stiffness are in the same arbitrary unit). Therefore the lamellipodium is able to reach its final destination by avoiding or displacing obstacles (Fig. 11B). When the lamellipodium can exert forces up to 2, it can displace all

obstacles and it will reach its final destination with a lower number of moves. Figure 11D shows the distribution of moves required to reach the final destination: as expected, a lamellipodium able to exert large forces will reach its final destination more rapidly.

DISCUSSION

Anatomical, biochemical and functional properties of growth cones and of their major components, lamellipodia and filopodia, have been thoroughly investigated (Aletta and Greene, 1988; Gomez and Letourneau, 1994; Baker and Macagno, 2007). The present work has two major aims: firstly, to examine in detail the kinetics and dynamics of filopodia and lamellipodia in an almost free environment and in a dense tissue; secondly, to provide a computational framework to rationalize the observed kinetics and dynamics.

Neurons process and compute information very efficiently, but during their entire lifespan, from the early stages of embryogenesis to adult neurogenesis, they also move, migrate and exert forces. Therefore, neurons not only process information but they also continuously perform and solve mechanical computations. In what follows, we will review several properties of the kinetics and dynamics of filopodia and lamellipodia and we will introduce and discuss the notion of mechanical computation.

EXPLORATION IN A FREE ENVIRONMENT

Growth cones explore the surrounding space through filopodia motion. Filopodia cannot exert forces larger than 2-3 pN (Kovar and Pollard, 2004; Footer et al., 2007; Cojoc et al., 2007) and therefore sense the environment in a gentle and delicate way. An optimal exploration requires an even sampling of the environment in space and time. As shown in Figure 2, filopodia explore the free space evenly, within 10 μm from the peripheral zone of the lamellipodium laterally and within 2-3 μm vertically. This nearly optimal exploration is caused by an orchestrated growth and retraction of neighboring filopodia (Figs. 3-4) and by their ability to lift up their tips. This orchestration of filopodia growth and retraction constitutes also an optimization of the available resources in which actin monomers are recycled from one filopodium to a neighboring one (Dent and Gertler, 2003; Medeiros et al., 2006) and consumption of ATP does not undergo large fluctuations with an excessive demand at specific times.

Filopodia have an average length of about 7 μm, occasionally extending up to 18 μm (Figs. 2 and 6) and are primarily composed by actin filaments. If the length between the tip and the base of an actin filament is significantly longer than its persistence length λ_P, then the tip and base will act almost independently and it will be nearly impossible to control the motion of the tip by acting on the base. In order to have a good control over the tip of a filopodium, its length must be comparable to λ_P, which for actin filaments is around 9 μm (Isambert et al., 1995). These considerations suggest that the average length of exploring filopodia is close to λ_P as experimentally observed.

EXPLORATION AND NAVIGATION IN A DENSE MEDIUM

It is well known that spines are continuously formed and pruned in the developing and mature brain (Engert and Bonhoeffer, 1999; Maletic-Savatic et al., 1999; Ahmari and Smith, 2002; Fonseca et al., 2006) and it is not surprising that filopodia growth and retraction can also occur in a dense medium, such as a dense neuronal culture (Fig. 6). Hippocampal filopodia move at a speed (0.06±0.04 μm/s) approximately 5-8 times slower than DRG filopodia in a free environment (0.4±0.3 μm/s). Filopodia exploration in a dense tissue is restricted along specific paths where the local density of biological material is less pronounced.

When two exploring growth cones come close, they quickly establish several contacts (Fig. 5), which are maintained even when one growth cone retracts. These contacts are likely to be primarily mediated by adhesion molecules, such as the neuroligins and their binding partners, the neurexins, the B ephrins and their partners EphR, etc (Yamagata et al., 2003; Cline and Haas, 2008). These contacts are only structural and not yet functional: the formation of synapses is a much longer process

occurring on a time scale of several hours (Nagerl et al., 2007; Cline and Haas, 2008). During long term potentiation, a sophisticated biochemical and genetic program is activated, but the insertion of new biological structures in synapses and dendrites requires a careful mechanical computation performed by the actin network and controlling proteins (Cingolani and Goda, 2008).

The migration of neurons in the developing brain or during adult neurogenesis necessitates the generation of larger forces: the force generated by a migrating keratocyte is of the order of 1-2nN (Prass et al., 2006), i.e. 10-100 times larger than the maximal force measured in a differentiating neuron (Cojoc et al., 2007). During morphogenesis, neuronal precursor cells migrate from the zone where they were born to their final destinations, which are often several millimeters away (Solecki et al., 2006; Ghashghaei et al., 2007) and in doing so, they must produce a substantial force and power. The dynamics of filopodia and lamellipodia are particularly interesting in densely packed tissue and it will be important to determine whether they show similar behaviors as those observed in our analysis *in vitro*, and whether mechanical forces of the same magnitude are generated and play an important role in the insertion of new cells into, for example, the hippocampus or the cortex. It is difficult to measure with optical tweezers and/or Atomic Force Microscopy the force exerted by exploring filopodia in a dense tissue. As the molecular mechanisms controlling force generation in isolated neurons and in neurons embedded in a tissues are expected to be the same or similar, forces per unit area exerted by filopodia and lamellipodia in the brain are expected to be of the order of tens pN μm^{-2}.

The fraction of the volume explored by hippocampal filopodia in a dense culture (Fig. 6) is about 10 times less than that explored by DRG filopodia (Fig. 2) in an almost free environment. This difference could be due to the fact that DRG are peripheral sensory neurons while hippocampal neurons are from the central nervous system and have different membrane receptors and motor proteins. In addition, DRG neurons are plated on a glass coated with poly-L-lysine while hippocampal neurons grow on top of other cells, hence their growth cones move on or within the extracellular matrix.

INTERACTION WITH OBSTACLES

When exploring, filopodia and lamellipodia often encounter obstacles and their reaction appears to follow stereotyped patterns (Fig. 8). After collision, an isolated filopodium either completely retracts, or partially retracts and branches new filopodia, or lightly collides with the obstacle and continues its growth. Similarly, a lamellipodium either collides with the obstacle and continues its motion by growing underneath it, or removes it in a "shovel like" fashion, or retracts. We have not been able to determine when and how a given reaction is chosen or decided and we propose that the choice is the result of a random process leading to a trial and error procedure. These reactions are likely to be mediated by receptors located at the filopodia and lamellipodia tips, such as the integrins, which are coupled to the cytoskeleton acting as signaling transducers and also helping the neuron to attach to the extracellular matrix or to other cells (Hynes, 2002).

MECHANICAL COMPUTATION: A PERSPECTIVE

The specific examples of mechanical computation illustrated in this manuscript can be addressed and studied from a molecular perspective. This requires a careful identification of all proteins and enzymes involved and a detailed analysis of the metabolic consumption occurring at each step (Mogilner and Oster, 1996; Carlsson, 2001; Carlsson, 2003; Janson et al., 2003; Mogilner and Rubinstein, 2005; Mogilner, 2006; Kerssemakers et al., 2006), which is beyond the scope of this article. Besides, it is also essential to understand the global computational plan in a more abstract form, as illustrated in Figures 9-11. Two factors seem to be at the basis of mechanical computation: an exploratory search relying on a trial and error strategy and a set of efficient feedback loops and/or simple reactions mediated by a variety of receptors and local protein networks, as discussed in the previous sections. The overall computation will not be deterministic and its accuracy, timing and performance will depend on the efficiency of the feedback loops, as illustrated in Figure 10.

Fundamental functions of the nervous system, such as parallel and information processing, require the solution of mechanical problems, which have not yet been addressed from a computational point of view. Let us consider, for instance, neuronal plasticity and memory formation, which are at

the basis of higher brain functions. One of the simplest mechanisms underlying memory formation is spine enlargement and the insertion of new receptors in its membrane. The motion of these receptors is primarily driven by random fluctuations (Triller and Choquet, 2008) caused by Brownian collisions with water molecules. In this case, the diffusive dynamics is constrained by specific molecular interactions so that molecules find their targets in a time scale compatible with the appropriate occurrence of biological events. Spine enlargement and the insertion of new receptors require the assembly of actin filaments, the transportation of new proteins from their synthesis sites, the generation of forces to open the way to the growing spine and many other steps. These biological events occur in a physical environment where forces are exerted and energy is consumed and these events necessitate the solution of mechanical problems that require sophisticated timing and planning. The understanding of these issues from a computational perspective is one of the aspects of mechanical computation.

Many problems of mechanical computation can be addressed with well known tools from Complexity Theory and Computational Geometry (Hopcroft et al., 2006) and are likely to be very similar to those addressed in Robotics (Xie, 2003). The exploration of an unknown environment by a random search is a strategy that is found very often in nature: indeed, it is used by insects and worms for food search, navigation, homing (Poggio and Reichardt, 1973; Valente et al., 2007) and also by mammals such as mice during maze exploration and other behavioral tasks (Drai et al., 2000). Finally, it is important to remember that random searches are also used in Computer Science to solve very difficult issues, such as finding global minima in optimization problems (Kirkpatrick et al., 1983) and finding approximate solutions for NP-complete problems (Boseniuk and Ebeling, 1988; Accardi and Ohya, 2004).

REFERENCES

Accardi L, Ohya M, 2004. A stochastic limit approach to the SAT problem. Open Sys. & Information Dyn. 11: 219-233, 2004.

Ahmari SE, Smith SJ. 2002. Knowing a nascent synapse when you see it. Neuron 34:333-336.

Aletta JM, Greene LA. 1988. Growth cone configuration and advance: a time-lapse study using video-enhanced differential interference contrast microscopy. J Neurosci 8:1425-1435.

Atilgan E, Wirtz D, Sun SX. 2006. Mechanics and dynamics of actin-driven thin membrane protrusions. Biophs J 90:65-76.

Baker MW, Kauffman B, Macagno ER, Zipser B. 2003. *In vivo* dynamics of CNS sensory arbor formation: a time-lapse study in the embryonic leech. J. Neurobiol 56:41-53.

Baker MW, Macagno ER. 2007. *In vivo* imaging of growth cone and filopodial dynamics:evidence for contact-mediated retraction of filopodia leading to the tiling of sibling processes. J Comp Neurol 500:850-862.

Bonifazi P, Ruaro ME, Torre V. 2005. Statistical properties of information processing in neuronal networks. European Journal of Neuroscience 22:11 2953-2964.

Boseniuk T, Ebeling W. 1988. Optimization of NP-Complete problems by Boltzmann-Darwin strategies including life cycles. Europhys. Lett. 6 107-112

Bray D, Thomas C, Shaw G. 1978. Growth cone formation in cultures of sensory neurons. Proc Natl Acad Sci USA 75:5226-5229.

Bustamante C, Macosko JC, Wuite GJ. 2000. Grabbing the cat by the tail: manipulating molecules one by one. Nat Rev Mol Cell Biol 1:130-136.

Carlsson AE. 2001. Growth of branched actin networks against obstacles. Biophys J 81:1907-1923.

Carlsson AE. 2003. Growth velocities of branched actin networks. Biophys J 84:2907-2918

Cingolani LA, Goda Y. 2008. Actin in action: the interplay between actin cytoskeleton and synaptic efficacy. Nat. Rev. Neurosci. 9:5, 344-56.

Cline H, Haas K. 2008. The regulation of dendritic arbor development and plasticity by glutamatergic synaptic input: a review of the synaptotrophic hypothesis. J. Physiol 586:1509-1518.

Cojoc D, Difato F, Ferrari E, Shahapure RB, Laishram J, Righi M, Di Fabrizio EM, Torre V. 2007. Properties of the force exerted by filopodia and lamellipodia and the involvement of cytoskeletal components. PLoS ONE 2(10):e1072. doi:10.1371/journal.pone.0001072.

Curinga G, Smith GM. 2007. Molecular/genetic manipulation of extrinsic axon guidance factors for CNS repair and regeneration. Experimental Neurology 209 (2008) 333–342.

Dai J, Sheetz MP. 1995. Mechanical properties of neuronal growth cone membranes studied by tether formation with laser optical tweezers. Biophys J 68:988-996.

Dayan P, Abbott LF. 2001. Theoretical neuroscience: computational and mathematical modeling of neural systems. Cambrdige, Mass. MIT Press c2001. ISBN 0-262-04199-5. Chapter 4: Information theory.

Dennerll TJ, Lamoureux P, Buxbaum RE, Heidemann SR. 1989. The cytomechanics of axonal elongation and retraction. J Cell Biol. 1989 Dec;109.

Dent E.W. Gertler, F. B. 2003. Cytoskeletal dynamics and transport in growth cone motility and axon guidance. Neuron 40:209-227.

Dent EW, Kalil K. 2001. Axon branching requires interactions between dynamic microtubules and actin filaments. J Neurosci 21:9757-9769.

Drai D, Benjamini Y, Golani I. 2000. Statistical discrimination of natural modes of motion in rat exploratory behavior. J Neurosci Methods. 96(2):119-31.

Duncan M, Fothergil T, Pujic Z, Richards LJ, Goodhill, GJ. 2008. Growth cone chemotaxis. Trends. Neurosci. 31:90-98. doi:10.1016/j.tins.2007.11.008

Engert F, Bonhoeffer T. 1999. Dendritic spine changes associated with hippocampal long-term synaptic plasticity. Nature 399:66-70.

Fonseca R, Nagerl UV, Bonhoffer T. 2006. Neuronal activity determines the protein synthesis dependence of long-term potentiation. Nat. Neuroscience 9:478-480.

Footer MJ, Kerssemakers JW, Theriot JA, Dogterom M. 2007. Direct measurement of force generation by actin filament polymerization using an optical trap. Proc Natl Acad Sci USA 104:2181-2186.

Forscher P, Smith SJ. 1988. Actions of cytochalasins on the organization of actin filaments and microtubules in a neuronal growth cone. J. Cell Biol., Oct 1988; 107: 1505 - 1516.

Galbraith CG, Yamada KM, Galbraith JA. 2007. Polymerizing actin fibers position integrins primed to probe for adhesion sites. Science 315:992-995.

Gallo G, Letourneau PC. 2000. Neurotrophins and the dynamic regulation of the neuronal cytoskeleton. J Neurobiol 44:159-173.

Gehler S, Shaw AE, Sarmiere PD, Bamburg JR, Letourneau PC. 2004. Brain-derived neurotrophic factor regulation of retinal growth cone filopodial dynamics is mediated through actin depolymerizing factor/cofilin. J Neurosci 24:10741-10749.

Ghashghaei HT, Lai C, Anton ES. 2007. Neuronal migration in the adult brain: are we there yet? Nat Rev Neurosci 8:141-151.

Gomez TM, Letourneau PC. 1994. Filopodia initiate choices made by sensory neuron growth cones at laminin/fibronectin borders *in vitro*. J Neurosci 14:5959-5972.

Goodman CS. 1996. Mechanisms and molecules that control growth cone guidance. Annu Rev Neurosci 19:341-377.

Gordon-Weeks PR. 2004. Microtubules and growth cone function. J Neurobiol 58:70-83.

Goslin K, Banker G. 1998. Culturing nerve cells. 2nd ed. Cambridge, MA: MIT Press. Rat hippocampal neurons in low-density culture, p 339-370.

Grunwald IC, Klein R. 2002. Axon guidance: receptor complexes and signaling mechanisms. Curr Opin Neurobiol 12:250-259.

Guan KL, Rao Y. 2003. Signalling mechanisms mediating neuronal responses to guidance cues. Nat Rev Neurosci 4:941-956.

Heidemann SR, Wirtz D. 2004. Towards a regional approach to cell mechanics. Trends Cell Biol. Volume 14, Issue 4, 1 April 2004, Pages 160-166. doi:10.1016/j.tcb.2004.02.003

Hopcroft, JE, Motwani R & Ullman JD. 2006. Introduction to Automata Theory, Languages and Computation. 3rd ed. Addison-Wesley Eds. New York.

Howard J. 2001. Mechanics of Motor Proteins and the Cytoskeleton. Sinauer Associates, Inc., Sunderland, MA. 384 pages.

Huber AB, Kolodkin AL Ginty DD, Cloutier JF. 2003. Signaling at the growth cone: ligand-receptor complexes and the control of axon growth and guidance. Annu Rev Neurosci 26:509-563.

Hynes R, 2002. Integrins: Bidirectional, Allosteric Signaling Machines. Cell, Volume 110, Issue 6, Pages 673-687.

Isambert H, Venier P, Maggs AC, Fattoum A, Kassab R, Pantaloni D, Carlier MF. 1995. Flexibility of actin filaments derived from thermal fluctuations. Effect of bound nucleotide, phalloidin, and muscle regulatory proteins. J. Biol. Chem. 270: 11437-11444.

Janson ME, de Dood ME, Dogterom M. 2003. Dynamic instability of microtubules is regulated by force. J Cell Biol 161:1029-1034.

Joshi HC, Chu D, Buxbaum RE, Heidemann SR. 1985. Tension and compression in the cytoskeleton of PC12 neurites. J. Cell Biol., Sep 1985; 101: 697 - 705.

Kerssemakers JW, Munteanu EL, Laan L, Noetzel TL, Janson ME, Dogterom M. 2006. Assembly dynamics of microtubules at molecular resolution. Nature 442:709-712.

Kirkpatrick S, Gelatt CD Jr & Vecchi MP. 1983. Optimization by Simulated Annealing. Science 220:671-680.

Koch C, Poggio T, Torre V. 1983. Nonlinear interactions in a dendritic tree: localization, timing and role in information processing. Proc. Natl. Acad. Science 80(9):2799-2802.

Koch C, Poggio T. 1983. A theoretical analysis of electrical properties of spines. Proc. Roy. Soc Lond. B 22:455-77.

Köhrmann M, Haubensak W, Hemraj I, Kaether C, Leβmann VJ, Kiebler MA. 1999. Fast, convenient, and effective method to transiently transfect primary hippocampal neurons. J Neurosci Res 58:831-835.

Kovar DR, Pollard TD. 2004. Insertional assembly of actin filament barbed ends in association with formins produces piconewton forces. Proc Natl Acad Sci USA 101:14725-14730.

Lebrand C, Dent EW, Strasser GA, Lanier LM, Krause M, Svitkina TM, Borisy GG, Gertler FB. 2004. Critical role of Ena/VASP proteins for filopodia formation in neurons and in function downstream of netrin-1. Neuron 2004, 42:37-49.

Lettvin JY, Maturana HR, McCulloch WS, Pitts WH. 1959. What the frog's eye tells the frog's brain. Proceedings of the IRE 47:11 pp 1940-1951.

Maletic-Savatic M, Malinow R, Svoboda K. 1999. Rapid dendritic morphogenesis in CA1 hippocampal dendrites induced by synaptic activity. Science 283:1923-1927.

McCulloch WS, Pitts WA. 1943. A logical calculus of the ideas immanent in nervous activity. Bull. Math. Biophys 5:115−133.

Medeiros NA, Burnette DT, Forscher P. 2006. Myosin II functions in actin-bundle turnover in neuronal growth cones. Nat. Cell. Biol 8:215-226.

Mogilner A, Oster G. 1996. Cell motility driven by actin polymerization. Biophys J 71:3030-3045.

Mogilner A, Rubinstein B. 2005. The physics of filopodial protrusion. Biophys J 89:782-795.

Mogilner A. 2006. On the edge: modeling protrusion. Curr Opin Cell Biol. 18(1):32-9.

Mongiu AK, Weitzke EL, Chaga OY, Borisy GG. 2007. Kinetic-structural analysis of neuronal growth cone veil motility. J Cell Sci 120:1113-1125.

Nagerl UV, Kostinger G, Anderson JC, Martin KA, Bonhoffer T. 2007. Protracted synaptogenesis after activity-dependent spinogenesis in hippocampal neurons. J. Neuroscience 27(30): 8149-56.

Neuman KC, Block SM. 2004. Optical trapping. Rev Sci Instrum 75:2787-2809.

Nicholls JG, Martin AR, Wallace BG, Fuchs PA. 2001. From Neuron to Brain. 4th ed. Washington: Sinauer Associates, Inc.

Pampaloni F, Lattanzi G, Alexandr Jonas A, Surrey T, Frey E, Florin E-L. 2006. Thermal fluctuations of grafted microtubules provide evidence of a length-dependent persistence length. PNAS 2006;103;10248-10253; doi:10.1073/pnas.0603931103

Poggio, T, Reichardt W. 1973. A theory of the pattern induced flight orientation of the fly Musca domestica. Kybernetyk 12(4. 185-203.

Pollard TD, Blanchoin L, Mullins RD. 2000. Molecular mechanisms controlling actin filament dynamics in nonmuscle cells. Annu Rev Biophys Biomol Struct 29:545-576.

Prass M, Jacobson K, Mogilner A, Radmacher M. 2006. Direct measurement of the lamellipodial protrusive force in a migrating cell. J Cell Biol 174:767-772.

Schaefer AW, Kabir N, Forscher P. 2002. Filopodia and actin arcs guide the assembly and transport of two populations of microtubules with unique dynamic parameters in neuronal growth cones. J. Cell Biol. 158:139-152.

Solecki DJ, Govek EE, Hatten ME. 2006. mPar6 alpha controls neuronal migration. J Neurosci 26:10624-10625.

Song H, Poo M. 2001. The cell biology of neuronal navigation. Nat Cell Biol 3:E81-E88.

Rohrbach A, Tischer C, Neumayer D, Florin E-L, Stelzer EHK. 2004. Trapping and tracking of a local probe with the photonic force microscope. Rev of Sci Instr 75(6): 2197-2210.

Triller A, Choquet D. 2008. New concepts in Synaptic Biology Derived from Single-Molecule Imaging. Neuron 59: 359-374

Valente D, Golani I, Mitra PP. 2007. Analysis of the trajectory of *Drosophila melanogaster* in a circular open field arena. PLoS ONE. Oct 24; 2(10):e1083.

Yamagata M, Sanes JR, Weiner JA. 2003. Synaptic adhesion molecules. Curr. Opin. Cell. Biol. 15(5):621-632.

Xie M. 2003. Fundamentals of robotics: linking perception to action. (Series in Machine Perception and Artificial Intelligence). World Scientific. ISBN-13:9789812383358